Generalized positivity constraint on magnetic equivalent layers

André L. A. Reis[1], Vanderlei C. Oliveira Jr.[1], and Valéria C. F. Barbosa[1]

ABSTRACT

It is known from the potential theory that a continuous and planar layer of dipoles can exactly reproduce the total-field anomaly produced by arbitrary 3D sources. We have proven the existence of an equivalent layer having an all-positive magnetic-moment distribution for the case in which the magnetization direction of this layer is the same as that of the true sources, regardless of whether the magnetization of the true sources is purely induced or not. By using this generalized positivity constraint, we have developed a new iterative method for estimating the total magnetization direction of 3D magnetic sources based on the equivalent-layer technique. Our method does not impose a priori information about the shape or the depth of the sources, does not require regularly spaced data, and presumes that the sources have a uniform magnetization direction. At each iteration, our method performs two steps. The first step solves a constrained linear inverse problem to estimate a positive magnetic-moment distribution over a discrete equivalent layer of dipoles. We consider that the equivalent sources are located on a plane and have a uniform and fixed magnetization direction. In the second step, we use the estimated magnetic-moment distribution and solve a nonlinear inverse problem for estimating a new magnetization direction for the dipoles. The algorithm stops when the equivalent layer yields a total-field anomaly that fits the observed data. Tests with synthetic data simulating different geologic scenarios show that the final estimated magnetization direction is close to the true one. We apply our method to field data from the Goiás alkaline province, over the Montes Claros complex, in the center of Brazil. The results suggest the presence of intrusions with remarkable remanent magnetization, in agreement with the current literature for this region.

INTRODUCTION

Most magnetic methods require knowledge of the magnetization direction and otherwise yield unsatisfactory interpretations of the exploration targets. This fact has propelled the development of several techniques for estimating magnetization direction over the past 50 years. Strategies for estimating this quantity can be divided into two main groups. The first one comprises the methods that presume a priori information about the shape of geologic sources. The iterative method presented by Bhattacharyya (1966) presumes that the magnetic source has a rectangular prismatic shape. Emilia and Massey (1974) approximate a seamount by a set of stacked prisms with uniform magnetization direction and variable magnetization intensity. Parker et al. (1987) represent the geometry of a seamount by using a covering of triangular facets and estimate the internal magnetization closest to a uniform solution. Medeiros and Silva (1995)

present a method that estimates the total magnetization direction and the spatial orientation of an isolated source having three orthogonal planes of symmetry. Ryuji and Uchiyama (2005) also approximate a seamount by a set of juxtaposed prisms, but they estimate a magnetization direction for each one. Finally, Oliveira et al. (2015) approximate the magnetic sources by spherical bodies with known centers for estimating their magnetization directions.

The second group is formed by methods that do not presume any information about the shape of the magnetic sources. Fedi et al. (1994), for example, propose a method that determines the best magnetization direction among a set of tentative values used to perform successive reductions to the pole (RTPs) in the Fourier domain. Phillips (2005) uses Helbig's integral for estimating the components of the magnetic-moment vector. Caratoni Tontini and Pedersen (2008) extend the Phillips' method by using the same Helbig's integral to estimate the magnetization direction and its

magnitude, also providing information about the position of the center of magnetization distribution. Lelièvre and Oldenburg (2009) develop a method for estimating the magnetization direction in complex geologic scenarios. Their method approximates the subsurface by a grid of juxtaposed prisms and estimates the components of the magnetization vector for each prism. In addition, there are methods based on the correlation of potential-field quantities (Dannemiller and Li, 2006; Gerovska et al., 2009; Liu et al., 2015; Zhang et al., 2018; Ribeiro-Filho et al., 2020).

Estimating the magnetization direction is extremely important not only for interpretation but also for processing the total-field anomaly data. One technique in the spatial domain commonly used for processing potential-field data is the equivalent layer. It was first introduced in exploration geophysics by Dampney (1969) and Emilia and Massey (1974) for processing gravity and magnetic data, respectively. After these pioneering works, this technique has been widely used for computing interpolation (Cordell, 1992; Mendonça and Silva, 1994; Barnes and Lumley, 2011; Siqueira et al., 2017), upward (or downward) continuation (Cribb, 1976; Hansen and Miyazaki, 1984; Li and Oldenburg, 2010; Mastellone et al., 2014), RTP (Silva, 1986; Leão and Silva, 1989; Guspí and Novara, 2009; Oliveira Jr. et al., 2013), the amplitude of the anomalous field (Li and Li, 2014), and for denoising gradient data (Martinez and Li, 2016). The equivalent-layer technique consists of approximating the observed data by those produced by a layer of discrete sources (e.g., prisms, dipoles, or point masses), which are commonly known as equivalent sources. The data produced by this fictitious layer (the equivalent layer) are commonly called predicted data.

In scanning magnetic microscopy, the equivalent-layer technique is generally used for interpreting the magnetic-moment distribution within thin planar sections of rock samples. Note that, in this case, the equivalent layer resembles the true source (a thin section of rock). Weiss et al. (2007) present one of the first works using the equivalent-layer technique in scanning magnetic microscopy. They point out without proof that the estimated magnetic-moment distribution on the layer is all-positive when the magnetization direction of the equivalent sources is equal to that used for artificially magnetizing the rock sample. Baratchart et al. (2013) show mathematically that, assuming a uniform magnetization direction within the thin section, the inverse problem of estimating the magnetic-moment distribution has a unique solution. Lima et al. (2013) propose a method in the frequency domain to investigate solutions having a uniform magnetization direction equal to that of a thin section of a geologic sample. They show empirically that, in this case, the estimated magnetic-moment distribution on the layer is entirely positive.

In geophysical exploration, the equivalent-layer technique is predominantly used for processing potential-field data. Under this perspective, there is no relationship between the physical-property distribution on the equivalent layer and the true geologic sources. Hence, the layer is just a mathematical abstraction devoid of geologic meaning. Few authors in the geophysical exploration literature have addressed the use of the equivalent-layer technique for interpreting geologic sources. Pedersen (1991), for example, discusses the relationship between the potential field and the equivalent source. Medeiros and Silva (1996) and Silva et al. (2010) estimate an apparent-magnetization map on a layer by using Tikhonov and entropic regularizations, respectively. Siqueira et al. (2017) establish a relationship between the excess of mass estimated over the equivalent layer and the true one. Li et al. (2014) prove, by using

a Fourier-domain approach, the existence of an all-positive magnetic-moment distribution over the layer and use this to overcome the RTP low-latitude instability. However, this work considers only the particular case in which the magnetic sources have a purely induced magnetization.

Here, we prove mathematically that there exists an all-positive magnetic-moment distribution within the equivalent layer even in the presence of geologic sources with remanent magnetization. This all-positive magnetic-moment distribution exists for all cases in which the magnetization directions of the equivalent sources have the same orientation as that of the true geologic sources, regardless of whether the magnetization of the true sources is purely induced or not. Grounded on this generalized positivity constraint, we present a new iterative method that uses the equivalent-layer technique for estimating the uniform magnetization direction of arbitrary sources by inverting the total-field anomaly data. Our method does not presume any information about the shape of the sources. At each iteration, our method solves (1) a linear inverse problem, subject to a positivity constraint, for estimating the magnetic-moment distribution within a planar equivalent layer of dipoles, and (2) a nonlinear inverse problem for estimating the uniform magnetization direction of the equivalent sources. Tests with synthetic data generated by different geologic scenarios show that the estimated magnetization direction converges to that of the true sources. We also applied our method to field data from the Goiás alkaline province (GAP), over the Montes Claros complex, in the center of Brazil. Our results are in agreement with those obtained independently by Zhang et al. (2018) in the same area, suggesting the presence of a remarkable remanent magnetization and showing the good performance of our method in interpreting a complex geologic scenario.

METHODOLOGY

Fundamentals of the magnetic equivalent layer and the positive magnetic-moment distribution

Let $\Delta T(x, y, z)$ be the total-field anomaly produced by a set of magnetic sources at a point (x, y, z) referred to in a topocentric Cartesian coordinate system with the x-, y-, and z-axes being oriented to the north, east, and down, respectively. Consider that the main geomagnetic field has a constant inclination I_0 and declination D_0 throughout the study area, so that its direction can be defined by the unit vector

$$\hat{\mathbf{F}}_0 = \begin{bmatrix} \cos I_0 \cos D_0 \\ \cos I_0 \sin D_0 \\ \sin I_0 \end{bmatrix}. \tag{1}$$

Additionally, consider that the magnetic sources have a constant total magnetization direction defined by the unit vector

$$\hat{\mathbf{m}}(\mathbf{q}) = \begin{bmatrix} \cos I \cos D \\ \cos I \sin D \\ \sin I \end{bmatrix}, \tag{2}$$

where the constants I and D represent its inclination and declination, respectively, and $\mathbf{q}$ is a 2×1 vector given by

$$\mathbf{q} = \begin{bmatrix} I \\ D \end{bmatrix}. \tag{3}$$

For convenience, we call $\mathbf{q}$ the magnetization direction vector. In this case, the total-field anomaly $\Delta T(x, y, z)$ can be written as follows:

$$\Delta T(x, y, z) = \hat{\mathbf{F}}_0^{\mathrm{T}} \mathbf{M}(x, y, z) \hat{\mathbf{m}}(\mathbf{q}), \qquad (4)$$

where $\mathbf{M}(x, y, z)$ is a matrix given by

$$\mathbf{M}(x, y, z) = \begin{bmatrix} \partial_{xx}\Gamma(x, y, z) & \partial_{xy}\Gamma(x, y, z) & \partial_{xz}\Gamma(x, y, z) \\ \partial_{xy}\Gamma(x, y, z) & \partial_{yy}\Gamma(x, y, z) & \partial_{yz}\Gamma(x, y, z) \\ \partial_{xz}\Gamma(x, y, z) & \partial_{yz}\Gamma(x, y, z) & \partial_{zz}\Gamma(x, y, z) \end{bmatrix}, \qquad (5)$$

with elements $\partial_{\alpha\beta}\Gamma(x, y, z) \equiv \frac{\partial^2 \Gamma(x,y,z)}{\partial\alpha\partial\beta}$, $\alpha, \beta = x, y, z$ representing the second derivatives of the harmonic function

$$\Gamma(x, y, z) = \gamma_m \iiint_v \frac{m(x', y', z')dv'}{[(x - x')^2 + (y - y')^2 + (z - z')^2]^{\frac{1}{2}}}. \qquad (6)$$

In this equation, $\gamma_m = 10^{-9}\mu_0/4\pi$ (in H/m); μ_0 is the vacuum magnetic permeability; and x', y', and z' are the coordinates of the volume element dv', which has total-magnetization intensity of $m(x', y', z')$ (in A/m) and is located within the volume v of the magnetic sources. We consider that the total-magnetization intensity $m(x', y', z')$ is strictly positive at all points within the magnetic sources. Consequently, $\Gamma(x, y, z)$ is positive at all points located outside the magnetic sources. From the mathematical point of view, $\mathbf{M}(x, y, z)$ (equation 5) and $\Gamma(x, y, z)$ (equation 6) resemble, respectively, the gradient tensor and the corresponding pseudogravitational potential that would be produced by the magnetic sources, at the point (x, y, z), if they had a density distribution proportional to $m(x', y', z')$. Notice that $\mathbf{M}(x, y, z)$ is symmetric, its trace is identically zero at all points (x, y, z) outside the magnetic sources, and it has five independent components that are themselves harmonic functions (Pedersen and Rasmussen, 1990). By exploring these properties, we can conveniently rewrite the total-field anomaly $\Delta T(x, y, z)$ (equation 4) as a linear combination of five independent harmonic functions as follows:

$$\Delta T(x, y, z) = a_{xx}\partial_{xx}\Gamma(x, y, z) + a_{xy}\partial_{xy}\Gamma(x, y, z)$$
$$+ a_{xz}\partial_{xz}\Gamma(x, y, z) + a_{yy}\partial_{yy}\Gamma(x, y, z) + a_{yz}\partial_{yz}\Gamma(x, y, z), \qquad (7)$$

where

$$a_{xx} = m_x F_x - m_z F_z$$
$$a_{xy} = m_x F_y + m_y F_x$$
$$a_{xz} = m_x F_z + m_z F_x$$
$$a_{yy} = m_y F_y - m_z F_z$$
$$a_{yz} = m_y F_z + m_z F_y \qquad (8)$$

are constants defined by the elements F_α and m_β, $\alpha = x, y, z$, $\beta = x, y, z$ of the vectors $\hat{\mathbf{F}}_0$ (equation 1) and $\hat{\mathbf{m}}(\mathbf{q})$ (equation 2), respectively. For simplicity, we have omitted the dependence on the parameters I_0 and D_0 (equation 1) and I and D (equation 2).

Let $\Delta\tilde{T}(x, y, z)$ be the total-field anomaly produced by a continuous layer of dipoles that have constant magnetization direction defined by the unit vector $\hat{\mathbf{m}}(\mathbf{q})$ (equation 3) and are located at the constant depth z_c. The total-field anomaly produced by this fictitious layer may be defined as

$$\Delta\tilde{T}(x, y, z) = \hat{\mathbf{F}}_0^{\mathrm{T}} \tilde{\mathbf{M}}(x, y, z) \hat{\mathbf{m}}(\mathbf{q}), \qquad (9)$$

where $\tilde{\mathbf{M}}(x, y, z)$ is a matrix given by

$$\tilde{\mathbf{M}}(x, y, z) = \begin{bmatrix} \partial_{xx}\Phi(x, y, z) & \partial_{xy}\Phi(x, y, z) & \partial_{xz}\Phi(x, y, z) \\ \partial_{xy}\Phi(x, y, z) & \partial_{yy}\Phi(x, y, z) & \partial_{yz}\Phi(x, y, z) \\ \partial_{xz}\Phi(x, y, z) & \partial_{yz}\Phi(x, y, z) & \partial_{zz}\Phi(x, y, z) \end{bmatrix}, \qquad (10)$$

with elements $\partial_{\alpha\beta}\Phi(x, y, z) \equiv \partial^2 \Phi(x, y, z)/\partial\alpha\partial\beta$, $\alpha, \beta = x, y, z$ representing the second derivatives of the harmonic function

$$\Phi(x, y, z) = \gamma_m \int_{-\infty}^{+\infty} \int_{-\infty}^{+\infty} \frac{p(x'', y'', z_c)dS''}{[(x - x'')^2 + (y - y'')^2 + (z - z_c)^2]^{\frac{1}{2}}},$$
$$z_c > z. \qquad (11)$$

In this equation, x'', y'', and z_c are the coordinates of the area element dS'', which has magnetic moment per unit area defined by the function $p(x'', y'', z_c)$ (in A). Note that $\tilde{\mathbf{M}}(x, y, z)$ (equation 10) also represents a gradient tensor (Pedersen and Rasmussen, 1990) and, consequently, it is symmetric, its trace is identically zero at all points (x, y, z) above the layer (with $z < z_c$), and it has five independent components that are themselves harmonic functions. These properties also permit rewriting $\Delta\tilde{T}(x, y, z)$ (equation 9) as a linear combination of independent harmonic functions given by

$$\Delta\tilde{T}(x, y, z) = a_{xx}\partial_{xx}\Phi(x, y, z) + a_{xy}\partial_{xy}\Phi(x, y, z)$$
$$+ a_{xz}\partial_{xz}\Phi(x, y, z) + a_{yy}\partial_{yy}\Phi(x, y, z) + a_{yz}\partial_{yz}\Phi(x, y, z), \qquad (12)$$

with coefficients $a_{\alpha\beta}$, $\alpha = x, y$, $\beta = x, y, z$ defined by equation 8.

We know from potential theory that it is possible to find a function $p(x'', y'', z_c)$ (equation 11) so that the condition $\Delta T(x, y, z) = \Delta\tilde{T}(x, y, z)$ holds true for all points (x, y, z) located above the fictitious layer of dipoles. In this case, the layer is called the *equivalent layer*. To investigate the properties of $p(x'', y'', z_c)$, we must first observe that, by imposing the aforementioned condition and using equations 7 and 12, we obtain

$$a_{xx}[\partial_{xx}\Phi(x, y, z) - \partial_{xx}\Gamma(x, y, z)]+$$
$$a_{xy}[\partial_{xy}\Phi(x, y, z) - \partial_{xy}\Gamma(x, y, z)]+$$
$$a_{xz}[\partial_{xz}\Phi(x, y, z) - \partial_{xz}\Gamma(x, y, z)]+$$
$$a_{yy}[\partial_{yy}\Phi(x, y, z) - \partial_{yy}\Gamma(x, y, z)]+$$
$$a_{yz}[\partial_{yz}\Phi(x, y, z) - \partial_{yz}\Gamma(x, y, z)] = 0, \quad z < z_c, \qquad (13)$$

where the coefficients $a_{\alpha\beta}$ (equation 8), $\alpha = x, y, z$, $\beta = x, y, z$ are defined by arbitrary values of I_0 and D_0 (equation 1) and I and D (equation 2). Because equation 13 is valid for any possible values of $a_{\alpha\beta}$, which are defined for any values of I_0, D_0, I, and D, the five linearly independent harmonic functions in brackets must be iden-

tically zero for all points (x, y, z) above the equivalent layer, where $z < z_c$. By equating each independent function to zero and rewriting the second derivatives of the surface integral $\Phi(x, y, z)$ (equation 11), we get

$$\partial_{\alpha\beta}\Gamma(x,y,z) = \int_{-\infty}^{+\infty}\int_{-\infty}^{+\infty} p(x'',y'',z_c)\partial_{\alpha\beta}\frac{1}{r}dS'', \quad z_c > z, \tag{14}$$

where (x'', y'', z_c) is a point on the equivalent layer and $\partial_{\alpha\beta}(1/r) \equiv (\partial^2/\partial\alpha\partial\beta)(1/r)$ represents the second derivative, with respect to $\alpha = x, y$ and $\beta = x, y, z$, of the inverse distance function

$$\frac{1}{r} \equiv \frac{1}{[(x - x'')^2 + (y - y'')^2 + (z - z_c)^2]^{\frac{1}{2}}}. \tag{15}$$

A possible solution for equation 14 can be obtained by deriving both sides of

$$\Gamma(x,y,z) = \int_{-\infty}^{+\infty}\int_{-\infty}^{+\infty} p(x'',y'',z_c)\frac{1}{r}dS'', \quad z_c > z. \tag{16}$$

Notice that the function $p(x'', y'', z_c)$ that solves this integral equation for $\Gamma(x, y, z)$ (equation 16) also solves the integral equations for the second derivatives $\partial_{\alpha\beta}\Gamma(x, y, z)$ (equation 14). It can be shown (see Appendix A) that equation 16 has a solution

$$p(x'',y'',z_c) = \frac{1}{2\pi}\partial_z\Gamma(x'',y'',z_c), \tag{17}$$
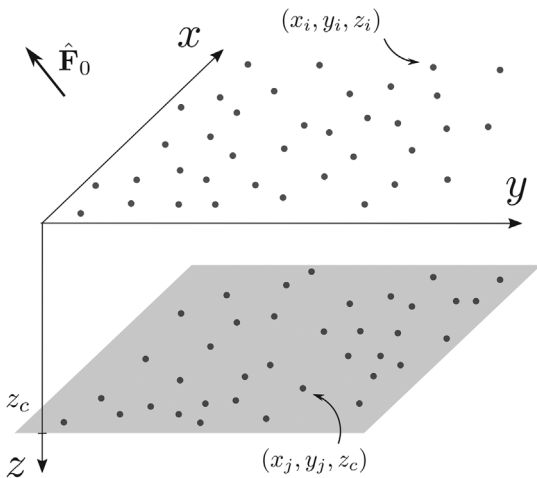

Figure 1. Schematic representation of an equivalent layer. The layer is positioned over the horizontal plane at a depth of $z = z_c$ (represented in gray), below the observation points (x_i, y_i, z_i), $i = 1, \ldots, N$. Each source is located at a point (x_j, y_j, z_c), $j = 1, \ldots, M$, and is represented by a dipole with unit volume, magnetization direction $\hat{\mathbf{m}}(\mathbf{q})$ (equation 2), and magnetic moment p_j (equation 19).

where, according to equation 6,

$$\partial_z\Gamma(x'',y'',z_c) = \gamma_m\int\int\int_v \frac{m(x',y',z')(z'-z_c)dv'}{[(x''-x')^2+(y''-y')^2+(z_c-z')^2]^{\frac{3}{2}}},$$
$$z' > z_c. \tag{18}$$

From the physical point of view, equation 18 represents the vertical component of the gravitational attraction (or the pseudogravity anomaly) that would be produced by the magnetic sources, on the equivalent layer, if they had a density distribution proportional to $m(x', y', z')$. Because $m(x', y', z')$ is strictly positive at all points (x', y', z') within the magnetic sources, $\partial_z\Gamma(x'', y'', z_c)$ is positive at all points (x'', y'', z_c) located on the equivalent layer.

The most interesting aspect of the magnetic-moment distribution $p(x'', y'', z_c)$ (equation 17) is that it is defined as the product of a positive constant $1/2\pi$ and the function $\partial_z\Gamma(x'', y'', z_c)$, which is strictly positive at all points (x'', y'', z_c) on the equivalent layer. Hence, $p(x'', y'', z_c)$ is strictly positive at all points on the equivalent layer as well. This relation is similar to that presented by Pedersen (1991) and Li et al. (2014). They determine, in the wavenumber domain, the magnetic-moment distribution within a continuous equivalent layer vertically magnetized by induction. They also consider a planar equivalent layer located below and parallel to a horizontal plane containing the observed total-field anomaly data. Under these assumptions, Pedersen (1991) and Li et al. (2014) conclude that the magnetic-moment distribution within the continuous equivalent layer is all positive and proportional to the pseudogravity anomaly produced by the source on the plane of the equivalent layer. Here, we do not follow the same wavenumber-domain reasoning used by those authors. Moreover, equation 17 generalizes this positivity condition because (1) it holds true for all cases in which the magnetization of the equivalent layer has the same direction as the true total-magnetization of the sources, whether it is purely induced or not, and (2) it does not require that the observed total-field anomaly data be on a plane.

Parametrization and forward problem

In practical situations, it is not possible to determine a continuous magnetic-moment distribution $p(x'', y'', z_c)$ (equation 17) over the equivalent layer. For this reason, the layer has to be approximated by a discrete set of dipoles (the equivalent sources) with the unit volume located at the constant depth $z = z_c$. The total-field anomaly produced by this discrete layer (the predicted total-field anomaly) at a given point (x_i, y_i, z_i), $i = 1, \ldots, N$ (Figure 1), is given by

$$\Delta T_i(\mathbf{s}) = \mathbf{g}_i(\mathbf{q})^{\mathrm{T}}\mathbf{p}, \tag{19}$$

where $\mathbf{s}$ is an $(M + 2) \times 1$ partitioned vector (the parameter vector) given by

$$\mathbf{s} = \begin{bmatrix} \mathbf{p} \\ \mathbf{q} \end{bmatrix}, \tag{20}$$

where $\mathbf{q}$ is the magnetization direction vector (equation 3); $\mathbf{p}$ is an $M \times 1$ vector (the magnetic-moment vector) whose jth element,

$j = 1, \ldots, M$, is the magnetic moment intensity p_j (in A m^2) of the jth dipole; and $\mathbf{g}_i(\mathbf{q})$ is another $M \times 1$ vector whose jth element is defined by the harmonic function

$$g_{ij}(\mathbf{q}) = \gamma_m \hat{\mathbf{F}}_0^T \mathbf{M}_{ij} \hat{\mathbf{m}}(\mathbf{q}). \tag{21}$$

In this equation, $\mathbf{M}_{ij}$ is a 3×3 matrix given by

$$\mathbf{M}_{ij} = \begin{bmatrix} \partial_{xx}\frac{1}{r} & \partial_{xy}\frac{1}{r} & \partial_{xz}\frac{1}{r} \\ \partial_{xy}\frac{1}{r} & \partial_{yy}\frac{1}{r} & \partial_{yz}\frac{1}{r} \\ \partial_{xz}\frac{1}{r} & \partial_{yz}\frac{1}{r} & \partial_{zz}\frac{1}{r} \end{bmatrix}, \tag{22}$$

where $\partial_{\alpha\beta}(1/r) \equiv (\partial^2/\partial\alpha\partial\beta)(1/r)$ represent the second derivatives, with respect to $\alpha = x, y, z$ and $\beta = x, y, z$, of the inverse distance $1/r$ (equation 15) between the coordinates of the observation points $(x, y, z) = (x_i, y_i, z_i)$ and the coordinates of the equivalent sources $(x'', y'', z_c) = (x_j, y_j, z_c)$ (Figure 1). Equations 19–22 show that the predicted total-field anomaly $\Delta T_i(\mathbf{s})$ has a linear relation with the magnetic-moment vector $\mathbf{p}$ and a nonlinear relation with the magnetization direction vector $\mathbf{q}$ (equation 3).

Inverse problem

Let $\Delta\mathbf{T}^o$ be the observed-data vector whose ith element ΔT_i^o is the observed total-field anomaly produced by the magnetic sources at the point (x_i, y_i, z_i), $i = 1, \ldots, N$ (Figure 1). Similarly, let $\Delta\mathbf{T}(\mathbf{s})$ be the predicted-data vector whose ith element $\Delta T_i(\mathbf{s})$ (equation 19) is the predicted total-field anomaly produced by the discrete equivalent layer at the same point (x_i, y_i, z_i). To estimate the parameter vector $\mathbf{s}$ (equation 20) minimizing the difference between $\Delta\mathbf{T}^o$ and $\Delta\mathbf{T}(\mathbf{s})$, we solve the following inverse problem:

$$\text{minimizing } \Psi(\mathbf{s}) = \|\Delta\mathbf{T}^o - \Delta\mathbf{T}(\mathbf{s})\|_2^2 + \mu f_0 \|\mathbf{p}\|_2^2, \tag{23a}$$

$$\text{subject to } \mathbf{p} \geq \mathbf{0}. \tag{23b}$$

On the right side of equation 23a, the first and second terms are the data-misfit function and the zeroth-order Tikhonov regularization function, μ is the regularizing parameter, $\|\cdot\|_2^2$ represents the squared Euclidean norm, and f_0 is a normalizing factor. This factor makes a trade-off between the data-misfit and zeroth-order Tikhonov regularization functions. In the inequality 23b, $\mathbf{0}$ is an $M \times 1$ vector with all elements equal to zero, and the inequality sign is applied element by element. This positivity constraint on the magnetic-moment vector $\mathbf{p}$ is incorporated by using the nonnegative least squares (NNLS) proposed by Lawson and Hanson (1974).

To solve this constrained inverse problem, let us first consider the following second-order expansion of the goal function (equation 23a) around $\mathbf{s} = \mathbf{s}^k$ (equation 20):

$$\Psi(\mathbf{s}^k + \Delta\mathbf{s}^k) \approx \Psi(\mathbf{s}^k) + \mathbf{J}^{kT}\Delta\mathbf{s}^k + \frac{1}{2}\Delta\mathbf{s}^{kT}\mathbf{H}^k\Delta\mathbf{s}^k, \tag{24}$$

where $\Delta\mathbf{s}^k$ is a perturbation on the parameter vector and the terms $\mathbf{J}^k$ and $\mathbf{H}^k$ are, respectively, the gradient vector and the Hessian matrix evaluated at $\mathbf{s}^k$. Then, we estimate the perturbation vector $\bar{\Delta}\mathbf{s}^k$ that

minimizes the expanded function (equation 24) by taking the gradient with respect to $\Delta\mathbf{s}^k$ and setting the result equal to the null vector. This procedure leads to the linear system

$$\mathbf{H}^k\bar{\Delta}\mathbf{s}^k = -\mathbf{J}^k, \tag{25}$$

which represents the kth step of the Gauss-Newton method (Aster et al., 2005) for minimizing our goal function (equation 23a). We rewrite this linear system by neglecting the cross-derivatives in the Hessian matrix as follows:

$$\begin{bmatrix} \mathbf{H}_{pp}^k & \mathbf{0} \\ \mathbf{0}^T & \mathbf{H}_{qq}^k \end{bmatrix} \begin{bmatrix} \bar{\Delta}\mathbf{p}^k \\ \bar{\Delta}\mathbf{q}^k \end{bmatrix} \approx - \begin{bmatrix} \mathbf{J}_p^k \\ \mathbf{J}_q^k \end{bmatrix}, \tag{26}$$

in which $\mathbf{0}$ is an $M \times 2$ matrix containing all of the elements equal to zero; $\bar{\Delta}\mathbf{p}^k = \bar{\mathbf{p}}^{k+1} - \bar{\mathbf{p}}^k$ is a correction on the magnetic-moment vector $\mathbf{p}$; $\bar{\Delta}\mathbf{q}^k = \bar{\mathbf{q}}^{k+1} - \bar{\mathbf{q}}^k$ is a correction on the magnetization direction $\mathbf{q}$; and the terms $\mathbf{J}_\alpha^k$ and $\mathbf{H}_{\alpha\alpha}^k$, $\alpha = p, q$ are the gradient vector and the Hessian matrix calculated with respect to the elements of $\mathbf{p}$ and $\mathbf{q}$, respectively. The gradient vector $\mathbf{J}_p^k$ and the Hessian matrix $\mathbf{H}_{pp}^k$ (equation 26) related to the magnetic-moment vector $\mathbf{p}$ (equation 20) are, respectively,

$$\mathbf{J}_p^k = -2\mathbf{G}_p^{kT}[\bar{\Delta}\mathbf{T}^o - \Delta\mathbf{T}(\bar{\mathbf{s}}^k)] + 2\mu f_0^k \bar{\mathbf{p}}^k \tag{27}$$

and

$$\mathbf{H}_{pp}^k = 2\mathbf{G}_p^{kT}\mathbf{G}_p^k + 2\mu f_0^k \mathbf{I}, \tag{28}$$

where $\mathbf{G}_p^k$ is an $N \times M$ matrix whose ijth element is given by the harmonic function $g_{ij}(\bar{\mathbf{q}}^k)$ (equation 21) evaluated at the magnetization direction $\bar{\mathbf{q}}^k$, $\mathbf{I}$ is the $M \times M$ identity matrix, and f_0^k is a normalizing factor equal to

$$f_0^k = \frac{\text{trace}(\mathbf{G}_p^{kT}\mathbf{G}_p^k)}{M}. \tag{29}$$

This factor is used with the purpose of making a trade-off between the terms forming the gradient vector $\mathbf{J}_p^k$ (equation 27) and the Hessian matrix $\mathbf{H}_{pp}^k$ (equation 28) along the iterative process. The gradient vector $\mathbf{J}_q^k$ and the Hessian matrix $\mathbf{H}_{qq}^k$ (equation 26) related to the magnetization direction $\mathbf{q}$ (equation 3) are, respectively,

$$\mathbf{J}_q^k = -2\mathbf{G}_q^{kT}[\Delta\mathbf{T}^o - \Delta\mathbf{T}(\bar{\mathbf{s}}^k)] \tag{30}$$

and

$$\mathbf{H}_{qq}^k \approx 2\mathbf{G}_q^{kT}\mathbf{G}_q^k, \tag{31}$$

in which $\mathbf{G}_q^k$ is an $N \times 2$ matrix given by

$$\mathbf{G}_q^k = \begin{bmatrix} \partial_I\mathbf{g}_1(\bar{\mathbf{q}}^k)^T\bar{\mathbf{p}}^k & \partial_D\mathbf{g}_1(\bar{\mathbf{q}}^k)^T\bar{\mathbf{p}}^k \\ \vdots & \vdots \\ \partial_I\mathbf{g}_N(\bar{\mathbf{q}}^k)^T\bar{\mathbf{p}}^k & \partial_D\mathbf{g}_N(\bar{\mathbf{q}}^k)^T\bar{\mathbf{p}}^k \end{bmatrix}, \tag{32}$$

where $\partial_\alpha\mathbf{g}_i(\bar{\mathbf{q}}^k) \equiv \partial\mathbf{g}_i(\bar{\mathbf{q}}^k)/\partial\alpha$, $\alpha = I, D$ represent the first derivatives of vector $\mathbf{g}_i(\bar{\mathbf{q}}^k)$ (equation 19) with respect to the incli-

nation I and the declination D of the total magnetization of the sources.

Iterative algorithm for solving the inverse problem

The iteration $k = 0$ of our algorithm starts with an initial guess $\bar{\mathbf{q}}^k = \bar{\mathbf{q}}^0$ for the direction vector $\mathbf{q}$ (equation 3). By using this $\bar{\mathbf{q}}^k$, the upper part of equation 26 leads to the following linear system for the magnetic-moment vector:

$$[\mathbf{G}_p^{k\mathrm{T}}\mathbf{G}_p^k + \mu f_0^k \mathbf{I}]\bar{\mathbf{p}}^k = \mathbf{G}_p^{k\mathrm{T}}\Delta\mathbf{T}^o. \qquad (33)$$

To impose the positivity constraint (equation 23b) on the magnetic-moment distribution $\bar{\mathbf{p}}^{k+1}$ within the equivalent layer, we solve this linear system (equation 33) by using the NNLS method (Lawson and Hanson, 1974; Silva Dias et al., 2007). This positive magnetic-moment distribution is then used to estimate a correction $\bar{\Delta}\mathbf{q}^k$ on the magnetization direction by solving the following unconstrained nonlinear system via the Levenberg-Marquardt method (Aster et al., 2005):

$$[\mathbf{G}_q^{k\mathrm{T}}\mathbf{G}_q^k + \lambda\mathbf{I}]\bar{\Delta}\mathbf{q}^k = \mathbf{G}_q^{k\mathrm{T}}[\Delta\mathbf{T}^o - \Delta\mathbf{T}(\mathbf{s}^k)], \qquad (34)$$

where λ is the Marquardt parameter and $\mathbf{I}$ is the identity matrix. After estimating the correction $\bar{\Delta}\mathbf{q}^k$ at the kth iteration, we update the magnetization direction as follows:

$$\bar{\mathbf{q}}^{k+1} = \bar{\mathbf{q}}^k + \bar{\Delta}\mathbf{q}^k, \qquad (35)$$

and we use it as input for estimating a new positive magnetic-moment distribution with equation 33 and so on. The iterative process stops when the goal function (equation 23a) is invariant along successive iterations. We show in Appendix B that our method fails if the sources are vertically magnetized.

Choice of layer depth z_c and regularization parameter μ

The procedure for the use of our methodology for estimating the total magnetization requires the choice of two main parameters. The first one is the layer depth z_c (Figure 1), and the second is the regularization parameter μ (equation 33).

There is a classic criterion proposed by Dampney (1969) to define the layer depth based on the horizontal data sampling. This criterion states that the distance between the plane containing the data and the plane defining the layer should vary from 2.5 to 6.0 times the horizontal data sampling. This criterion, however, is valid for evenly spaced data. Here, we define the layer depth z_c by using the horizontal space between adjacent flight lines of an airborne survey. We found empirically that z_c can vary from 2 to 3 times the spacing between adjacent flight lines. Notice that the range that we found empirically is smaller than that proposed by Dampney. Apparently, this is due to the fact that, in an airborne survey, the data sampling along the lines is smaller than the space between the lines.

To solve equation 33, we have to choose a reliable regularization parameter μ. For this purpose, we use the L-curve method (Hansen and O'Leary, 1993). This approach is widely used in the literature to find a regularizing parameter, which filters out enough noise without losing too much information in the final solution. The procedure of finding the parameter plots a curve of optimal values between the solution and residual norms. The corner of the curve is the optimal regularization parameter, which establishes a trade-off between the regularizing and data-misfit functions.

APPLICATION TO SYNTHETIC DATA

We applied the proposed method to three synthetic data sets simulating different geologic scenarios. The first one is generated by a model containing a set of multiple sources with different geometries, all of them with the same magnetization direction. The second is generated by a set of multiple magnetic bodies, but one of them is a shallow-seated source with the same magnetization direction. In the third test, we violate the hypothesis of unidirectional magnetization by simulating a shallow-seated source with a magnetization direction different from the other bodies.

In all of the tests, the simulated data were computed on a regular grid of 49×25 points (with a total of $N = 1225$ observations) at $z = -100$ m. The simulated area extends over 12 km along the x- and y-axes, resulting in a grid spacing of 250 and 500 m along the x- and y-axes, respectively. The data were contaminated with pseudorandom Gaussian noise with zero mean and 10 nT standard deviation. The geomagnetic field direction simulated was $I_0 = -40°$ and $D_0 = -22°$ for the inclination and declination, respectively. In the inversion, we use an equivalent layer composed by a grid of 49×25 dipoles (with a total of $M = 1225$ equivalent sources) positioned at a depth of $z_c = 1150$ m below the observation plane (2.5 times the greater grid spacing). We use the L-curve to choose the regularizing parameter (μ). Our algorithm starts with an initial guess $\bar{\mathbf{q}}^0 = (-10°, -10°)$ for the inclination and declination, respectively.

Unidirectional magnetization sources

We generate a 3D prism with a polygonal cross section whose top is positioned at a depth of 450 m and the bottom at 3150 m with a magnetization intensity of 4 A/m. We also generate two spheres with magnetization intensity equal to 3 A/m and radius equal to 500 m. The coordinates of the spheres' centers are $x_c = 1800$ m, $y_c = -1800$ m, and $z_c = 1000$ m and $x_c = 800$ m, $y_c = 800$ m, and $z_c = 1000$ m. We produce two rectangular prisms with 2.5 A/m of magnetization intensity. The smaller prism has the top at a depth of 450 m and side lengths of 1000, 700, and 500 m along the x-, y-, and z-axes, respectively. The greater prism has the top at a depth of 500 m and side lengths of 1000, 2000, and 1550 m along the x-, y-, and z-axes, respectively. The total magnetization of all simulated sources has inclination of $-25°$ and declination of 30°. The noise-corrupted data are shown in Figure 2a.

Figure 2b shows the predicted data produced by the equivalent layer. Figure 2c shows the residuals defined as the difference between the simulated data (Figure 2a) and the predicted data (Figure 2b). The residuals appear normally distributed with a mean of -0.29 nT and a standard deviation of 9.67 nT as shown in Figure 2d. The estimated magnetization direction $\bar{\mathbf{q}}$ has inclination of $-28.6°$ and declination of 30.7°, which are very close to the true values. Figure 2e shows the estimated magnetic-moment distribution $\bar{\mathbf{p}}$. The convergence of the algorithm is shown in Figure 2f. These results show that the all-positive magnetic-moment distribution and the estimated magnetization direction produce an acceptable data fitting.

Unidirectional magnetization with a shallow-seated source

Here, we test the methodology performance when a shallow-seated source exists. The model seems like the previous test except for the smaller prism, whose top is 150 m deep while maintaining its volume. The magnetization intensity of this shallow prism is equal to 1.5 A/m. The magnetization direction of all sources is −25° inclination and declination 30°, respectively. The synthetic data are shown in Figure 3a.

Figure 3b shows the predicted total-field anomaly produced by the equivalent layer. Figure 3c shows the residuals defined as the difference between the simulated data (Figure 3a) and the predicted data (Figure 3b). The residuals appear normally distributed with a mean of −0.42 nT and a standard deviation of 10.67 nT as shown in Figure 3d. Figure 3e shows the estimated magnetic-moment distribution $\bar{\mathbf{p}}$. The convergence of the algorithm is shown in Figure 3f. Despite the large residual located above the shallow-seated source, we consider that the methodology produced a reliable result because the estimated magnetization direction $\bar{\mathbf{q}}$ has inclination −28.8° and declination 31.7°, and it is very close to the corresponding true magnetization direction, and the all-positive magnetic-moment distribution produces an acceptable data fitting.

Shallow-seated source with a different magnetization direction

In this test, we simulate the presence of a shallow-seated body with a magnetization direction different from the other magnetic sources. The shallow prism has dimensions and magnetization intensity equal to the previous test. However, the magnetization direction of the shallow prism is 20° of inclination and −30° of declination, whereas the other sources have inclination −25° and declination 30°. The noise-corrupted data are shown in Figure 4a.

Figure 4b shows the predicted total-field anomaly. Figure 4c shows the residuals defined as the difference between the simulated data (Figure 4a) and the predicted data (Figure 4b). The residuals have a mean of −0.71 nT and a standard deviation of 12.84 nT as shown in Figure 4d. The estimated magnetization direction $\bar{\mathbf{q}}$ has inclination of −30.4° and declination of 27.6°. Figure 4e shows the estimated magnetic-moment distribution $\bar{\mathbf{p}}$. The convergence of the algorithm is shown in Figure 4f. We also note that the estimated magnetization direction is very close to the magnetization direction of most sources. Moreover, despite the slight difference from the true magnetization direction, the estimated magnetic-moment distribution produces an acceptable data fit. With the exception of the small area exactly above the small-seated prism, most of the residuals are close to 0 nT.
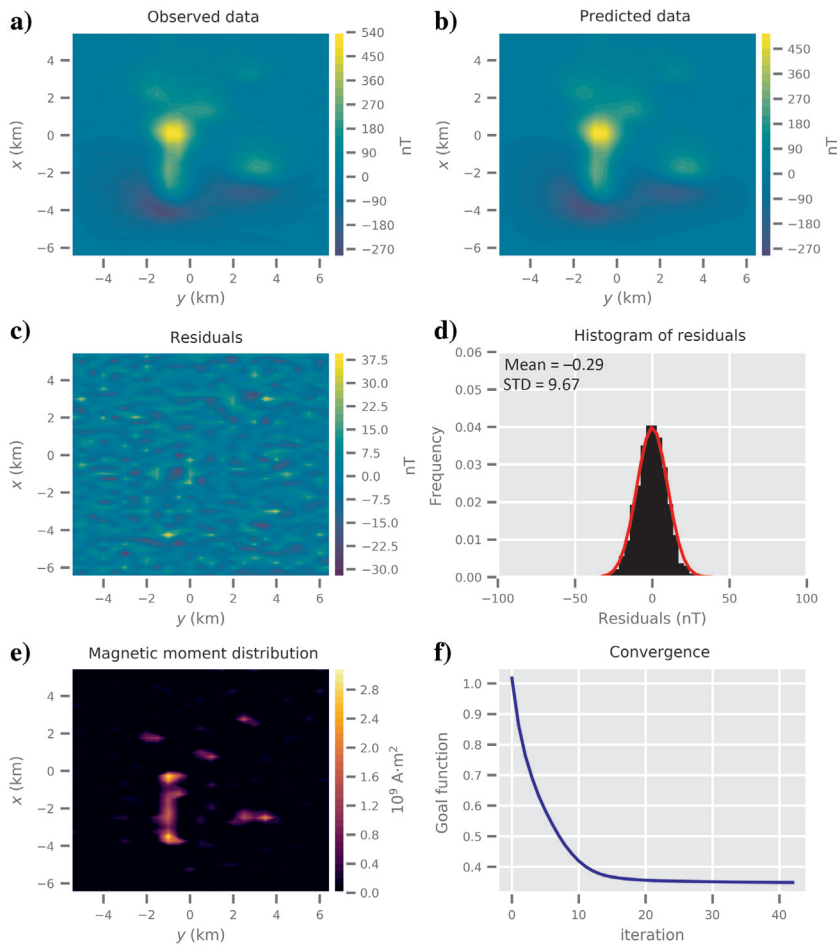

Figure 2. Application to synthetic data for multiple sources with unidirectional magnetization. (a) Noise-corrupted total-field anomaly. (b) Predicted data produced by the equivalent layer. (c) Difference between the data shown in (a and b). (d) Histogram of the residuals. (e) All-positive magnetic-moment distribution. (f) Goal function value (equation 23a) per iteration showing the convergence.

APPLICATION TO FIELD DATA

The GAP is a region in the central part of Brazil where there are occurrences of mafic-ultramafic alkaline magmatism. This region presents a variety of rocks with extensive petrographic types. Throughout the area, there are mafic-ultramafic complexes (plutonic intrusions), subvolcaninc alkaline intrusions (diatremes), and volcanic products (kamafugite lava flows) with several dikes. Some of the main alkaline complexes of GAP are the Montes Claros de Goiás, Diorama, Córrego dos Bois, Morro do Macaco, and Fazenda Buriti. These alkaline intrusions are surrounded by a Precambrian basement and the Phanerozoic sedimentary rocks of the Paraná Basin (Junqueira-Brod et al., 2005; Carlson et al., 2007; Marangoni and Mantovani, 2013; Dutra et al., 2014). Recent studies indicate the existence of a remarkable remanent magnetization component within these intrusions (Marangoni and Mantovani, 2013; Oliveira et al., 2015; Marangoni et al., 2016; Zhang et al., 2018).

The aeromagnetic survey has a flight pattern with north–south flight lines spaced from approximately 500 m and data acquired at intervals of approximately 8 m along each line, and a constant height of 100 m from the terrain. The geomagnetic field direction for this area was −19.5° and −18.5° for the inclination and declination, respectively. We invert the total-field anomaly (Figure 5a) from the alkaline complex of Montes Claros. To speed up data processing and inversion, we downsampled the data along the flight lines, resulting in a grid of 55 × 32 points (a total of $N = 1787$ ob-

servations). This new setup results in approximately 320 and 470 m grid spacing along the x- and y-axes, respectively. We use an equivalent layer composed by a grid of 55 × 32 dipoles (a total of $M = 1787$ equivalent sources) positioned at a depth of 840 m below the observation plane (approximately twice the greater grid spacing). The algorithm starts with an initial guess of −70° and 50° for the inclination and declination, respectively. Figure 5b shows the predicted data produced by the equivalent layer. Figure 5c shows the residuals defined as the difference between the observed data (Figure 5a) and the predicted data (Figure 5b). Note that the two small places in Figure 5c where large residuals are clearly apparent may indicate the existence of shallow-seated geologic sources with a different magnetization direction. However, the histogram of the residuals (Figure 5d) is acceptable with its mean of −15.79 nT (∼0.1% of the maximum value of the total-field anomaly data) and standard deviation of 339.04 nT (∼3% of the maximum value of the total-field anomaly data). The estimated magnetization direction $\bar{\mathbf{q}}$ has inclination of −45.5° and declination of 38.4°. Figure 5e and 5f shows the estimated magnetic-moment distribution $\bar{\mathbf{p}}$ and the convergence of the algorithm. We check the quality of the estimated magnetization direction by computing the RTP of the observed total-field anomaly. We can note that the RTP anomaly (Figure 6) exhibits predominantly positive values and decays to zero toward the borders of the study area. For this reason, we consider that the estimated magnetization direction led to a satisfactory RTP anomaly. We conclude with these results that the all-positive mag-

Figure 3. Multiple synthetic sources with a shallow-seated body under unidirectional magnetization. (a) Noise-corrupted total-field anomaly. (b) Predicted data produced by the equivalent layer. (c) Difference between the data shown in (a and b). (d) Histogram of the residuals. (e) All-positive magnetic-moment distribution. (f) Goal function value (equation 23a) per iteration showing the convergence.
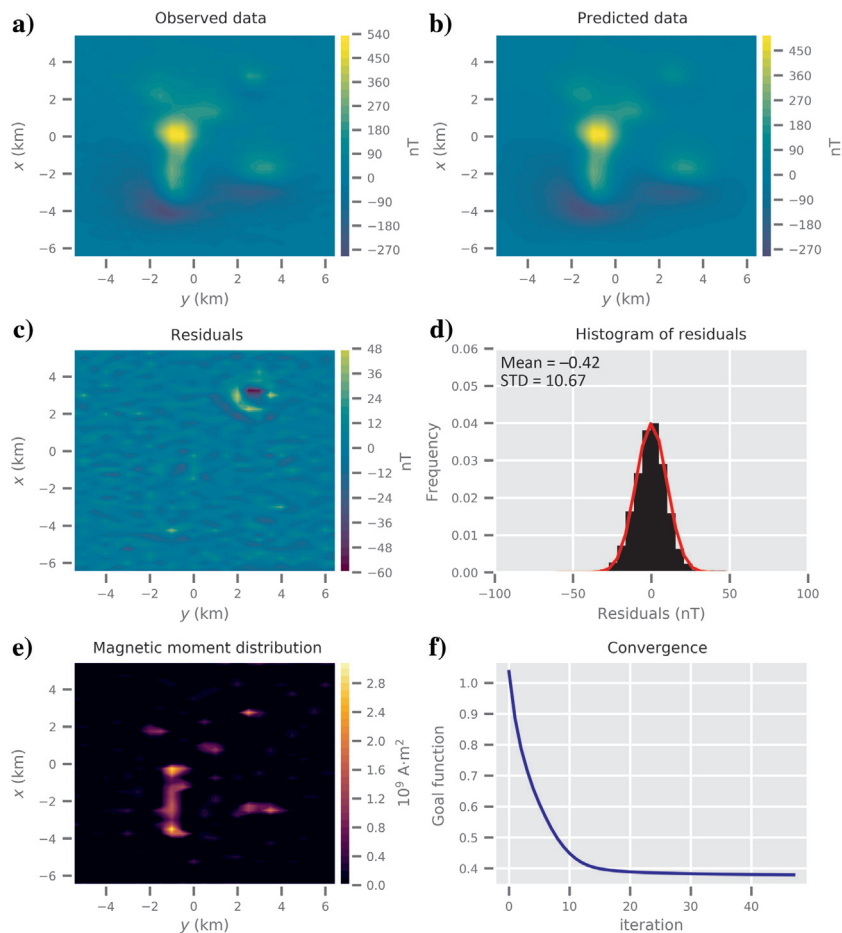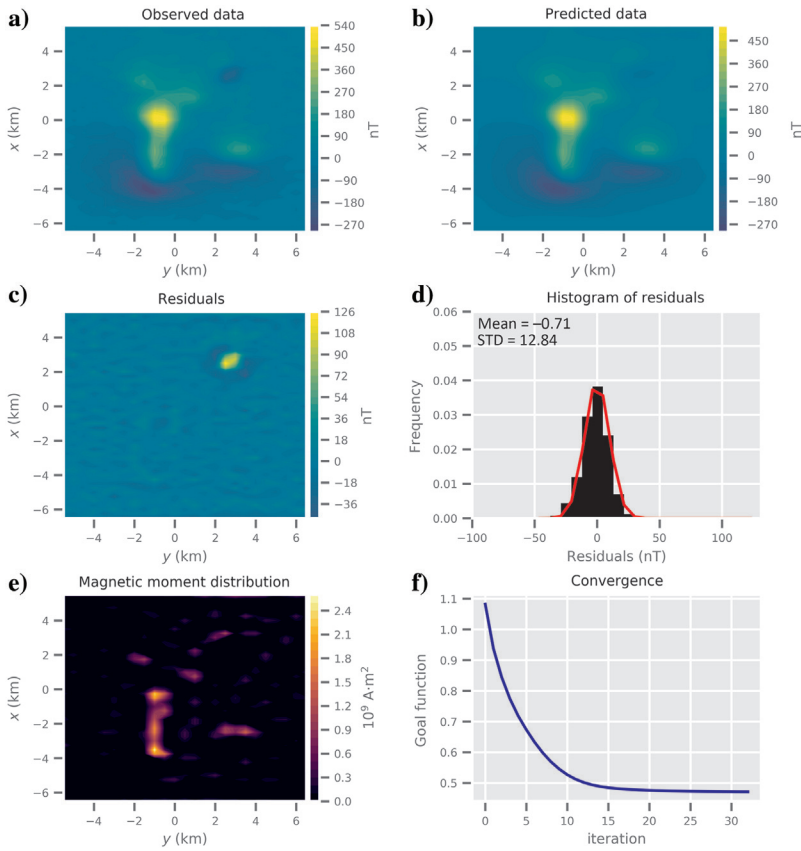
Figure 4. Multiple synthetic sources with a shallow-seated body under different magnetization directions. (a) Noise-corrupted total-field anomaly. (b) Predicted data produced by the equivalent layer. (c) Difference between the data shown in (a and b). (d) Histogram of residuals. (e) All-positive magnetic-moment distribution. (f) Goal function value (equation 23a) per iteration showing the convergence.
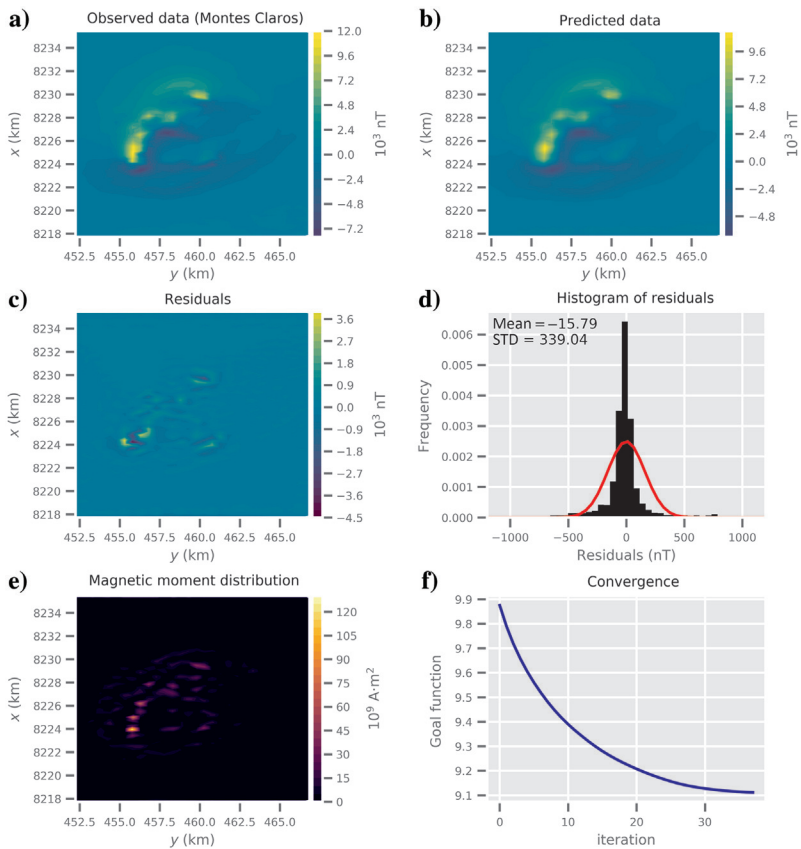
Figure 5. Application to field data from the alkaline complex of Montes Claros (Brazil). (a) Observed total-field anomaly. (b) Predicted data produced by the equivalent layer. (c) Difference between the data shown in (a and b). (d) Histogram of the residuals. (e) All-positive magnetic-moment distribution. (f) Goal function value (equation 23a) per iteration showing the convergence.
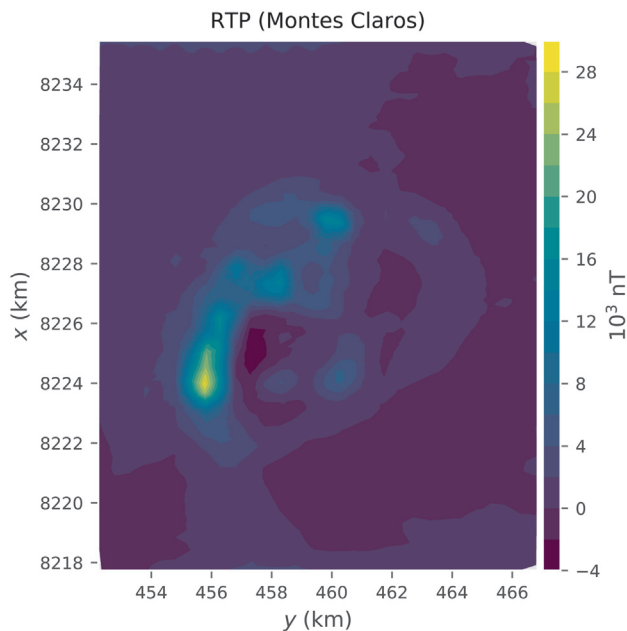
RTP (Montes Claros)

Figure 6. Application to field data from the alkaline complex of the Montes Claros (Brazil). The RTP anomaly computed by using the estimated magnetization distribution shown in Figure 5e.
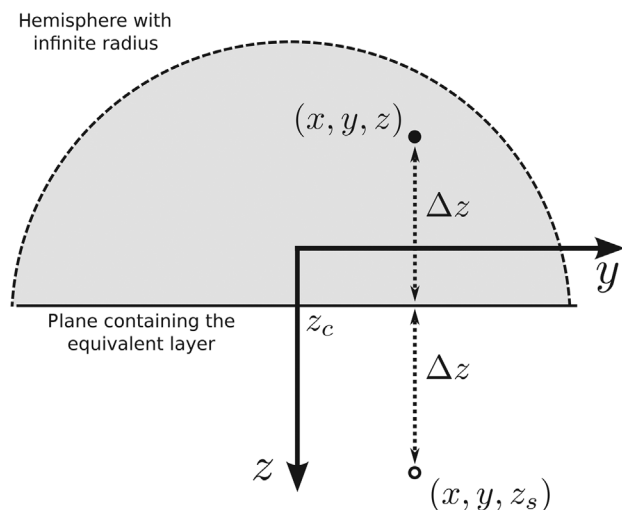
Figure 7. A 2D representation of the surface used for applying the Green's identities. The surface is formed by a hemisphere (the dashed line) with infinite radius and the plane $z = z_c$ containing the equivalent layer. The points (x, y, z) (the black dot) and (x, y, z_s) (the white dot) are symmetrically positioned with respect to the plane $z = z_c$ and are defined by $z = z_c - \Delta z$ and $z = z_c + \Delta z$, respectively.

netic moment distribution and the estimated magnetization direction produce an acceptable data fit. According to Marangoni and Mantovani (2013), laboratory measurements made with rock samples of the GAP indicate an average total magnetization direction with inclination and declination equal to $-39.0°$ and $1.0°$, respectively. However, Zhang et al. (2018) use aeromagnetic data to estimate a total magnetization direction with inclination of $-49.0°$ and declination of $46.0°$ for the same complex of Montes Claros de Goiás. These differences may be due to the fact that the results obtained with rock samples represent the total-magnetization direction of local shallow sources, whereas the result obtained with airborne data reflects the predominant influence of deeper sources at the study area. We note that our results, also obtained with airborne data, are very close to those obtained by Zhang et al. (2018) for the same complex. Moreover, they also confirm the existence of the remarkable remanent magnetization for this area.

CONCLUSION

We have mathematically proven that the total-field anomaly data caused by a set of magnetic sources with a uniform magnetization direction can be reproduced exactly by a continuous and planar layer of dipoles having an all-positive magnetic-moment distribution. This theoretical property holds true for the case in which a layer has the same magnetization direction as that of the true sources, regardless of whether they have a purely induced magnetization or not. By using this generalized positivity constraint, we presented a new iterative method for estimating the total magnetization direction of 3D magnetic sources based on the equivalent-layer technique. At each iteration, we impose a positivity constraint on the estimated magnetic-moment distribution of the layer and solve a nonlinear inverse problem for estimating the magnetization direction of the equivalent sources. Prior knowledge about the shape and depth of the magnetic sources is not required, neither is the use of an evenly spaced data set. This methodology can be applied for determining the magnetization direction of multiple sources, considering all of them with the same magnetization direction. Results obtained with synthetic data produced by multiple sources show that the estimated magnetization direction obtained by our iterative method successfully retrieves the true one. Tests with synthetic data illustrate how the presence of a relatively shallow-seated source affects the result obtained by our method for the cases in which it has a magnetization direction equal to and different from the other sources. In both cases, the equivalent layer yielded large data misfits above the shallow source; however, we cannot distinguish whether the shallow source has a magnetization direction equal to or different from the other sources. Moreover, our method produces the most poorly estimated magnetization direction when a shallow-seated source is magnetized in a direction that differs from the other sources. An application to field data over the Goiás alkaline province, in the center of Brazil, has confirmed that our method can be a reliable tool for interpreting complex geologic scenarios. The result over the Montes Claros complex suggests the presence of a strong remanent magnetization component and corroborates a previous study conducted independently at the same area. The estimated magnetic-moment distribution over the layer has led to a very acceptable RTP but also produced large data misfits at some isolated regions. We presume that these locally large data misfits are due to shallow sources; however, we cannot infer if they have the same magnetization direction as the other bodies.

ACKNOWLEDGMENTS

DATA AND MATERIALS AVAILABILITY

Data associated with this research are confidential and cannot be released.

APPENDIX A

DEDUCTION OF EQUATION 17

In this appendix, we prove the existence of an all-positive magnetic-moment distribution $p(x'', y'', z_c)$ that solves the integral shown in equation 16.

Consider a closed surface located above the magnetic sources, formed by the plane $z = z_c$ containing the equivalent layer and a hemisphere with infinite radius (Figure 7). This surface encloses a region where $\Gamma(x'', y'', z_c)$ (equation 6) is harmonic at all points. By using the Green's second identity (Kellogg, 1967, p. 215), we can show that

$$0 = \frac{1}{4\pi} \int_{-\infty}^{+\infty} \int_{-\infty}^{+\infty} \partial_z \Gamma(x'', y'', z_c) \frac{1}{\ell}$$
$$- \Gamma(x'', y'', z_c) \partial_z \frac{1}{\ell} dS'', \quad z_c > z, \quad (A-1)$$

where $\Gamma(x'', y'', z_c)$ is the volume integral defined by equation 6 and

$$\frac{1}{\ell} \equiv \frac{1}{\sqrt{(x-x'')^2 + (y-y'')^2 + (z_s - z_c)^2}} \quad (A-2)$$

is the inverse distance between the fixed point (x'', y'', z_c), located on the equivalent layer, and the point (x, y, z_s), with $z_s = z_c + \Delta z$, $\Delta z > 0$. The point (x, y, z_s) is conveniently defined as the mirror of (x, y, z), located at $z = z_c - \Delta z$, with respect to the plane $z = z_c$ containing the equivalent layer (Figure 7). Equation A-1 combined with the Green's third identity (Kellogg, 1967, p. 219) gives rise to

$$\Gamma(x, y, z) = \frac{1}{4\pi} \int_{-\infty}^{+\infty} \int_{-\infty}^{+\infty} \partial_z \Gamma(x'', y'', z_c)$$
$$\times \left(\frac{1}{r} + \frac{1}{\ell}\right) \Gamma(x'', y'', z_c) \left(\partial_z \frac{1}{r} + \partial_z \frac{1}{\ell}\right) dS'', \quad z_c > z, \quad (A-3)$$

where $1/r$ is defined by equation 15. The term $(1/r + 1/\ell)$ represents the *Green's function of the second kind* (Kellogg, 1967, p. 246) associated with this integral. We can verify that $1/r = 1/\ell$, $\partial_z(1/r) = -\partial_z(1/\ell)$ and, consequently,

$$\Gamma(x, y, z) = \frac{1}{2\pi} \int_{-\infty}^{+\infty} \int_{-\infty}^{+\infty} \partial_z \Gamma(x'', y'', z_c) \frac{1}{r} dS'', \quad z_c > z. \quad (A-4)$$

This equation shows the inherent ambiguity of potential field methods (Roy, 1962) and solves the *Neumann's problem* or the *sec-*

ond boundary value problem of potential theory (Kellogg, 1967, p. 246). In the present case, this problem consists of defining the harmonic function $\Gamma(x, y, z)$ (equation 6) at the region above the equivalent layer from the values of its vertical derivative on the plane containing the equivalent layer.

APPENDIX B

VERTICALLY MAGNETIZED SOURCES

Our method fails when the total magnetization of the sources has a direction equal or close to vertical. This appendix provides the theoretical basis for understanding this limitation.

Consider the limiting case in which the total magnetization of the sources is vertical (e.g., $I = \pm 90°$). In this case, the total-field anomaly $\Delta T(x, y, z)$ (equation 4) does not depend on the declination D, which reveals a well-known fact: vertically magnetized sources do not have a definite declination. As a consequence, the minimum region of the goal function (equation 23a) on the parameter space is not well defined; rather, it is elongated in the direction of D. Unfortunately, the positivity constraint on the magnetic-moment vector (equation 23b) does not solve this ambiguity with respect to the declination D.

To understand how this ambiguity affects our method, let us start by analyzing the $N \times 2$ matrix $\mathbf{G}_q^k$ (equation 32) required for estimating the correction $\bar{\Delta}\mathbf{q}^k$ in the magnetization direction (equation 34). Its ith line is defined by the dot product of the estimated magnetic-moment vector $\bar{\mathbf{p}}^k$ and the first derivatives $\partial_\alpha \mathbf{g}_i(\bar{\mathbf{q}}^k) \equiv \partial \mathbf{g}_i(\bar{\mathbf{q}}^k)/\partial\alpha$, $\alpha = I, D$, of the vector $\mathbf{g}_i(\mathbf{q})$ (equation 19), evaluated at $\mathbf{q} = \bar{\mathbf{q}}^k$, with respect to the inclination I and the declination D of the total magnetization of the sources. The jth element $\partial_\alpha g_{ij}(\bar{\mathbf{q}}^k) \equiv \partial g_{ij}(\bar{\mathbf{q}}^k)/\partial\alpha$ of the $M \times 1$ vector $\partial_\alpha \mathbf{g}_i(\bar{\mathbf{q}}^k)$ is defined by computing the derivative of the harmonic function $g_{ij}(\mathbf{q})$ (equation 21), as follows:

$$\partial_\alpha g_{ij}(\bar{\mathbf{q}}^k) = \gamma_m \hat{\mathbf{F}}_0^T \mathbf{M}_{ij} \partial_\alpha \hat{\mathbf{m}}(\bar{\mathbf{q}}^k), \quad \alpha = I, D, \quad (B-1)$$

where

$$\partial_I \hat{\mathbf{m}}(\bar{\mathbf{q}}^k) = \begin{bmatrix} -\sin \bar{I}^k \cos \bar{D}^k \\ -\sin \bar{I}^k \sin \bar{D}^k \\ \cos \bar{I}^k \end{bmatrix} \quad (B-2)$$

and

$$\partial_D \hat{\mathbf{m}}(\bar{\mathbf{q}}^k) = \begin{bmatrix} -\cos \bar{I}^k \sin \bar{D}^k \\ \cos \bar{I}^k \cos \bar{D}^k \\ 0 \end{bmatrix} \quad (B-3)$$

are derivatives of the unit vector $\hat{\mathbf{m}}(\mathbf{q})$ (equation 2), evaluated at the magnetization direction $\bar{\mathbf{q}}^k = [\bar{I}^k \bar{D}^k]^T$, with respect to I and D.

Notice that, as the estimated inclination $\bar{I}^k$ approaches $\pm 90°$, all elements forming the vector $\partial_D \hat{\mathbf{m}}(\bar{\mathbf{q}}^k)$ (equation B-3) and, consequently, those forming the second column of $\mathbf{G}_q^k$ (equation 32) tend to zero. As a result, the nonlinear problem for estimating the magnetization direction (equation 34) becomes insensitive to changes in the declination D, and the convergence of our method becomes very slow due to the flatness of the goal function $\Psi(\mathbf{s})$ (equation 23a) in the parameter space.

REFERENCES

Aster, R. C., B. Borchers, and C. H. Thurber, 2005, Parameter estimation and inverse problems (international geophysics): Academic Press.

Baratchart, L., D. P. Hardin, E. A. Lima, E. B. Saff, and B. P. Weiss, 2013, Characterizing kernels of operators related to thin-plate magnetizations via generalizations of Hodge decompositions: Inverse Problems, **29**, 015004, doi: 10.1088/0266-5611/29/1/015004.

Barnes, G., and J. Lumley, 2011, Processing gravity gradient data: Geophysics, **76**, no. 2, I33–I47, doi: 10.1190/1.3548548.

Bhattacharyya, B. K., 1966, A method for computing the total magnetization vector and the dimensions of a rectangular block shaped from magnetic anomalies: Geophysics, **31**, 74–96, doi: 10.1190/1.1439765.

Caratoni Tontini, F., and L. B. Pedersen, 2008, Interpreting magnetic data by integral moments: Geophysical Journal International, **174**, 815–824, doi: 10.1111/j.1365-246X.2008.03872.x.

Carlson, R. W., A. L. N. Araujo, T. C. Junqueira-Brod, J. C. Gaspar, J. A. Brod, I. A. Petrinovic, M. H. B. M. Hollanda, M. M. Pimentel, and S. Sichel, 2007, Chemical and isotopic relationships between peridotite xenoliths and maficultrapotassic rocks from southern Brazil: Chemical Geology, **242**, 415–434, doi: 10.1016/j.chemgeo.2007.04.009.

Cordell, L., 1992, A scattered equivalent-source method for interpolation and gridding of potential-field data in three dimensions: Geophysics, **57**, 629–636, doi: 10.1190/1.1443275.

Cribb, J., 1976, Application of the generalized linear inverse to the inversion of static potential data: Geophysics, **41**, 1365–1369, doi: 10.1190/1.1440686.

Dampney, C. N. G., 1969, The equivalent source technique: Geophysics, **34**, 39–53, doi: 10.1190/1.1439996.

Dannemiller, N., and Y. Li, 2006, A new method for determination of magnetization direction: Geophysics, **71**, no. 6, L69–L73, doi: 10.1190/1.2356116.

Dutra, A. C., Y. Marangoni, and R. I. F. Trindade, 2014, Aeromagnetic and physical-chemical properties of some complexes from Goiás Alkaline Province: Brazilian Journal of Geology, **44**, 361–373, doi: 10.5327/Z2317-4889201400030003.

Emilia, D. A., and R. L. Massey, 1974, Magnetization estimation for non-uniformly magnetized seamounts: Geophysics, **39**, 223–231, doi: 10.1190/1.1440423.

Fedi, M., G. Florio, and A. Rapolla, 1994, A method to estimate the total magnetization direction from a distortion analysis of magnetic anomalies: Geophysical Prospecting, **42**, 261–274, doi: 10.1111/j.1365-2478.1994.tb00209.x.

Gerovska, D., M. J. Araúzo-Bravo, and P. Stavrev, 2009, Estimating the magnetization direction of sources from southeast Bulgaria through correlation between reduced-to-the-pole and total magnitude anomalies: Geophysical Prospecting, **57**, 491–505, doi: 10.1111/j.1365-2478.2008.00761.x.

Guspí, F., and I. Novara, 2009, Reduction to the pole and transformations of scattered magnetic data using Newtonian equivalent sources: Geophysics, **74**, no. 5, L67–L73, doi: 10.1190/1.3170690.

Hansen, P., and D. O'Leary, 1993, The use of the L-curve in the regularization of discrete ill-posed problems: SIAM Journal on Scientific Computing, **14**, 1487–1503, doi: 10.1137/0914086.

Hansen, R. O., and Y. Miyazaki, 1984, Continuation of potential fields between arbitrary surfaces: Geophysics, **49**, 787–795, doi: 10.1190/1.1441707.

Junqueira-Brod, T. C., J. C. Gaspar, J. A. Brod, and C. V. Kafino, 2005, Kamafugitic diatremes: Their textures and field relationships with examples from the Goiás Alkaline Province, Brazil: Journal of South American Earth Sciences, **18**, 337–353, doi: 10.1016/j.jsames.2004.11.002.

Kellogg, O. D., 1967, Foundations of potential theory, reprint from the first edition of 1929 ed.: Springer-Verlag.

Lawson, C. L., and R. J. Hanson, 1974, Solving least squares problems: SIAM.

Leão, J. W. D., and J. B. C. Silva, 1989, Discrete linear transformations of potential field data: Geophysics, **54**, 497–507, doi: 10.1190/1.1442676.

Lelièvre, P. G., and D. W. Oldenburg, 2009, A 3D total magnetization inversion applicable when significant, complicated remanence is present: Geophysics, **74**, no. 3, L21–L30, doi: 10.1190/1.3103249.

Li, S.-L., and Y. Li, 2014, Inversion of magnetic anomaly on rugged observation surface in the presence of strong remanent magnetization: Geophysics, **79**, no. 2, J11–J19, doi: 10.1190/geo2013-0126.1.

Li, Y., M. Nabighian, and D. W. Oldenburg, 2014, Using an equivalent source with positivity for low-latitude reduction to the pole without striation: Geophysics, **79**, no. 6, J81–J90, doi: 10.1190/geo2014-0134.1.

Li, Y., and D. W. Oldenburg, 2010, Rapid construction of equivalent sources using wavelets: Geophysics, **75**, no. 3, L51–L59, doi: 10.1190/1.3378764.

Lima, E. A., B. P. Weiss, L. Baratchart, D. P. Hardin, and E. B. Saff, 2013, Fast inversion of magnetic field maps of unidirectional planar geological magnetization: Journal of Geophysical Research, Solid Earth, **118**, 2723–2752, doi: 10.1002/jgrb.50229.

Liu, S., X. Hu, Y. Xi, T. Liu, and S. Xu, 2015, 2D sequential inversion of total magnitude and total magnetic anomaly data affected by remanent magnetization: Geophysics, **80**, no. 3, K1–K12, doi: 10.1190/geo2014-0019.1.

Marangoni, Y., H. Zhang, and H. Ferreira, 2016, Gravity and magnetic integrated data interpretation of the Córrego dos Bois Complex, Goiás Alkaline Province, central Brazil: Revista Brasileira de Geofísica, **33**, 599–610, doi: 10.22564/rbgf.v33i4.756.

Marangoni, Y. R., and M. S. Mantovani, 2013, Geophysical signatures of the alkaline intrusions bordering the Paraná Basin: Journal of South American Earth Sciences, **41**, 83–98, doi: 10.1016/j.jsames.2012.08.004.

Martinez, C., and Y. Li, 2016, Denoising of gravity gradient data using an equivalent source technique: Geophysics, **81**, no. 4, G67–G79, doi: 10.1190/geo2015-0379.1.

Mastellone, D., M. Fedi, S. Ialongo, and V. Paoletti, 2014, Volume continuation of potential fields from the minimum-length solution: An optimal tool for continuation through general surfaces: Journal of Applied Geophysics, **111**, 346–355, doi: 10.1016/j.jappgeo.2014.10.020.

Medeiros, W. E., and J. B. C. Silva, 1995, Simultaneous estimation of total magnetization direction and 3-D spatial orientation: Geophysics, **60**, 1365–1377, doi: 10.1190/1.1443872.

Medeiros, W. E., and J. B. C. Silva, 1996, Geophysical inversion using approximate equality constraints: Geophysics, **61**, 1678–1688, doi: 10.1190/1.1444086.

Mendonça, C. A., and J. B. C. Silva, 1994, The equivalent data concept applied to the interpolation of potential field data: Geophysics, **59**, 722–732, doi: 10.1190/1.1443630.

Oliveira, V. C., Jr., V. C. F. Barbosa, and L. Uieda, 2013, Polynomial equivalent layer: Geophysics, **78**, no. 1, G1–G13, doi: 10.1190/geo2012-0196.1.

Oliveira, V. C., Jr., D. P. Sales, V. C. F. Barbosa, and L. Uieda, 2015, Estimation of the total magnetization direction of approximately spherical bodies: Nonlinear Processes in Geophysics, **22**, 215–232, doi: 10.5194/npg-22-215-2015.

Parker, R. L., L. Shure, and J. A. Hildebrand, 1987, The application of inverse theory to seamount magnetism: Reviews of Geophysics, **25**, 17–40, doi: 10.1029/RG025i001p00017.

Pedersen, L. B., 1991, Relations between potential fields and some equivalent sources: Geophysics, **56**, 961–971, doi: 10.1190/1.1443129.

Pedersen, L. B., and T. M. Rasmussen, 1990, The gradient tensor of potential field anomalies: Some implications on data collection and data processing of maps: Geophysics, **55**, 1558–1566, doi: 10.1190/1.1442807.

Phillips, D. J., 2005, Can we estimate total magnetization directions from aeromagnetic data using Helbig's integrals?: Earth, Planets and Space, **57**, 681–689, doi: 10.1186/BF03351848.

Ribeiro-Filho, N., R. Bijani, and C. Ponte-Neto, 2020, Improving the cross-correlation method to estimate the total magnetization direction vector of isolated sources: A space-domain approach for unstable inclination values: Geophysics, **85**, no. 4, J59–J70, doi: 10.1190/geo2019-0008.1.

Roy, A., 1962, Ambiguity in geophysical interpretation: Geophysics, **27**, 90–99, doi: 10.1190/1.1438985.

Ryuji, K., and A. Uchiyama, 2005, Three-dimensional magnetization vector inversion of a seamount: Earth, Planets and Space, **57**, 691–699, doi: 10.1186/BF03351849.

Silva, J. B. C., 1986, Reduction to the pole as an inverse problem and its application to low-latitude anomalies: Geophysics, **51**, 369–382, doi: 10.1190/1.1442096.

Silva, J. B. C., S. S. Vasconcelos, and V. C. F. Barbosa, 2010, Apparent-magnetization mapping using entropic regularization: Geophysics, **75**, no. 2, L39–L50, doi: 10.1190/1.3358160.

Silva Dias, F. J., V. C. Barbosa, and J. B. Silva, 2007, 2D gravity inversion of a complex interface in the presence of interfering sources: Geophysics, **72**, no. 2, I13–I22, doi: 10.1190/1.2424545.

Siqueira, F. C. L., V. C. Oliveira, Jr., and V. C. F. Barbosa, 2017, Fast iterative equivalent-layer technique for gravity data processing: A method grounded on excess mass constraint: Geophysics, **82**, no. 4, G57–G69, doi: 10.1190/geo2016-0332.1.

Weiss, B. P., E. A. Lima, L. E. Fong, and F. J. Baudenbacher, 2007, Paleomagnetic analysis using squid microscopy: Journal of Geophysical Research, Solid Earth, **112**, B09105, doi: 10.1029/2007JB004940.

Zhang, H., D. Ravat, Y. R. Marangoni, G. Chen, and X. Hu, 2018, Improved total magnetization direction determination by correlation of the normalized source strength derivative and the reduced-to-pole fields: Geophysics, **83**, no. 6, J75–J85, doi: 10.1190/geo2017-0178.1.